Available online at www.sciencedirect.com
SCIENCE DIRECT®
Comput. Methods Appl. Mech. Engrg. 192 (2003) 395–420
Computer methods in applied mechanics and engineering
www.elsevier.com/locate/cma

Robust integration schemes for flexible multibody systems

Olivier A. Bauchau [a,*], Carlo L. Bottasso [b], Lorenzo Trainelli [b]

[a] Georgia Institute of Technology, School of Aerospace Engineering, 270 Ferst Drive, Atlanta, GA 30332-0150, USA
[b] Dipartimento di Ingegneria Aerospaziale, Politecnico di Milano, Campus Bovisa, Via La Masa 34, 20138 Milano, Italy

Received 26 June 2002; received in revised form 26 June 2002

Abstract

A framework for the development of robust time integration schemes for nonlinear, flexible multibody systems is presented. The proposed schemes are designed to meet four specific requirements: nonlinear unconditional stability of the scheme, a rigorous treatment of both geometric and material nonlinearities, exact satisfaction of the constraints, and the presence of high frequency numerical dissipation. Specific algorithms are presented for rigid bodies, cables, beams, shells, and elasto-dynamics. The kinematic nonlinearities are treated in a rigorous manner for all elements, and the material nonlinearities can be handled when the constitutive laws stem from the existence of a strain energy density function. The treatment of the constraint equations associated with the six lower pair joints are presented as well. The efficiency and robustness of the proposed approach is demonstrated with specific numerical examples.

1. Introduction

The classical approach to the numerical simulation of flexible multibody systems proceeds in two steps: first, the equations of motion of the system are written in a convenient form, then general purpose differential algebraic equations (DAE) solvers are used to integrate these equations in the time domain. General purpose DAE integrators are specifically designed for effectively dealing with the dual differential/algebraic nature of the equations but are otherwise unaware of the specific features and characteristics of the equations being solved.

The equations governing nonlinear flexible multibody systems present very specific features. First, they are characterized by linear and rotational tensorial fields describing kinematic (displacements, velocities) and cokinematic (forces, momenta) quantities. Second, nonlinearities can arise from several sources: large displacements and finite rotations (geometric nonlinearities), or nonlinear constitutive laws for the deformable components of the system (material nonlinearities). Third, a distinguishing feature of multibody systems is the presence of joints which impose different types of kinematic constraints between the various bodies of the system. An exhaustive classification of these joint types can be found in text books, such as [1],

* Corresponding author. Fax: +1-404-894-2760.
E-mail address: olivier.bauchau@ae.gatech.edu (O.A. Bauchau).

0045-7825/03/$ - see front matter
PII: S0045-7825(02)00519-4

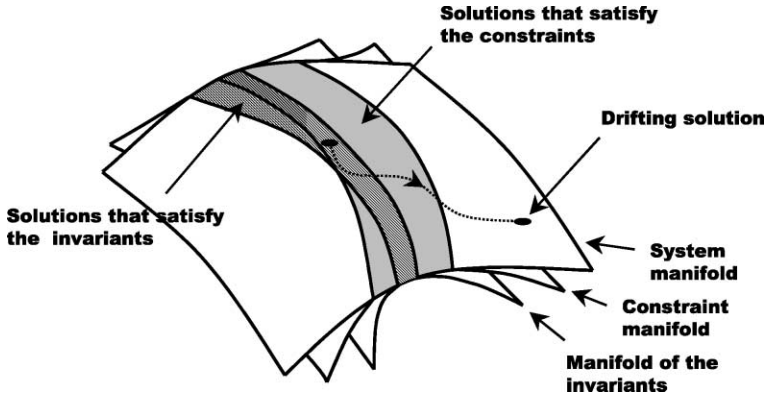

Fig. 1. System, constraint and invariant manifolds for a multibody system.

for instance. More often than not, constraints are modeled via the Lagrange multipliers technique that imposes the nonlinear algebraic constraints on the system. Fourth, the exact solution of the equations of motion implies the preservation of a number of dynamic invariants, such as energy and momenta. Consequently, the system response evolves on a special manifold, as depicted in Fig. 1 in a symbolic manner. Fifth, when the elastic bodies of the system are modeled by means of an appropriate spatial discretization process, such as the finite element method, high frequency modes are introduced in the system.

Present numerical procedures treat these features in various manners. While the geometric nonlinearities are dealt with in an exact manner in most approaches, the other features of the system are treated with various levels of accuracy. For example, index reduction methods [2] transform the holonomic constraints into velocity or acceleration constraints, thus introducing the drift phenomenon, i.e. the numerical solution is allowed to drift away from the level set defined by the holonomic constraints. Similarly, the preservation of the dynamic invariants, such as the system energy, is usually ignored. Here again, the numerical solution is allowed to drift away from the level set defined by the dynamic invariants. This situation is conceptually depicted in Fig. 1.

While standard approaches perform adequately for a number of simulations, problems can arise when modeling flexible, nonlinear multibody systems involving a large number of degrees of freedom. In this case, robust algorithms that satisfy precise *requirements* should be *designed* for the time integration of such systems. This paper describes an approach that satisfies the following requirements: *nonlinear unconditional stability* of the scheme, a *rigorous treatment of all nonlinearities*, the *exact satisfaction of the constraints*, and the presence of *high frequency numerical dissipation*. The proof of nonlinear unconditional stability stems from two physical characteristics of multibody systems that will be reflected in the numerical scheme: the preservation of the total mechanical energy, and the vanishing of the work performed by constraint forces. Numerical dissipation is obtained by letting the solution drift from the constant energy manifold in a controlled manner in such a way that at each time step, energy can be dissipated but not created. The rigorous integration on the system configuration manifold defined by the nature of finite rotations and the presence of constraints is akin to the concept of *geometric integration* proposed by several authors [3].

A general overview of the integration of DAE's and preservation of constraint manifolds can be found in Refs. [2,4,5]. The problem of nonlinear unconditional stability was discussed by Hughes [6], but the first practical schemes were developed by Simo and his coworkers. The case of rigid bodies is treated in Ref. [7], the extension to beams in [8], to shells in [9] and to nonlinear elasto-dynamics in [10]. The methodology was extended to multibody systems in Ref. [11]. Clearly, these *energy methods* are receiving increased attention, as the growing body of literature on the subject indicates.

Energy preserving (EP) algorithm achieve nonlinear unconditional stability because the numerical procedure preserves a positive definite quantity, the total mechanical energy of the system, at each step of the integration procedure. Nonlinear unconditional stability is the first step towards the development of robust algorithms, but does not guarantee, per se, satisfactory performance of the scheme. Indeed, the average acceleration scheme [12] is an EP scheme for linear systems. Yet, undesirable characteristics of this scheme were reported by Hughes [6]: in large systems, numerical round-off errors are sufficient to provide excitation of the high frequency modes of the system. This energy does not dissipate, due to the strict energy preservation characteristic of the algorithm. This prompted the development of algorithms presenting high frequency numerical dissipation in linear systems, such as the HHT scheme [13], later refined by the generalized-α method [14]. Although the HHT scheme has been successfully used for nonlinear flexible multibody systems [15], its stability and dissipative characteristics are established for linear systems only.

For nonlinear flexible multibody systems, EP schemes perform rather poorly when applied to complex simulations of engineering interest [11]. First, the time histories of internal forces and velocities can present a very significant high frequency content. Second, the presence of these high frequency oscillations hinders the convergence process for the solution of the nonlinear equations of motion. The selection of a smaller time step does not necessarily help this convergence process, as a smaller time step allows even higher frequency oscillations to be present in the response. These oscillations are particularly violent in multibody system simulations because these systems are rather stiff due to the presence of numerous algebraic constraints, and furthermore, the nonlinearities of the system provide a mechanism to transfer energy from the low to the high frequency modes. Hence, the presence of high frequency numerical dissipation is an indispensable feature of robust time integrators for multibody systems. It is all the more important in view of the fact that the high frequency content of the response is an artifact of the spatial discretization that contains no information about the physical behavior of the system. Note that high frequency dissipation should be an intrinsic property of the integrator, and it cannot be obtained from an *a-posteriori* filtering of the results.

In view of the requirements set forth, the following procedure for the simulation of nonlinear, flexible multibody systems is proposed. First, a discretization process for flexible members of the system is developed that preserves the total mechanical energy of the system at the discrete solution level. Then, a discretization process is proposed for the forces of constraint associated with the holonomic and nonholonomic constraints imposed on the system. Forces of constraint are discretized in a manner that guarantees the satisfaction of the nonlinear constraint manifold, i.e. the constraint condition will not drift. At the same time, the discretization implies the vanishing of the work performed by the forces of constraint at the discrete solution level. Consequently, the discrete energy conservation laws proved for the flexible members of the system are not upset by the introduction of the constraints. The resulting EP scheme provides nonlinear unconditional stability for nonlinear, flexible multibody systems. However, it clearly lacks the indispensable high frequency numerical dissipation required to tackle realistic engineering problems.

In a second phase, a new discretization, closely related to that of the EP scheme, is developed for the flexible components of the system. This new discretization implies a discrete energy decay statement that results in high frequency numerical dissipation. The discretization of the forces of constraint is also closely related to that of the EP scheme and presents identical properties: no drift of the constraint conditions and vanishing of the work they perform. Here again, the introduction of constraints does not upset the discrete energy decay law. The resulting energy decaying (ED) scheme satisfies all the design requirements set forth earlier, and is therefore ideally suited for the simulation of nonlinear, flexible multibody systems.

Similar ED schemes were proposed in Refs. [16–23]. In particular, Ref. [23] addressed the problem of rigid bodies and geometrically exact beams, and showed that slightly different EP and ED discretizations

can be developed, usually through different treatments or parameterizations of finite rotations. Some discretizations might present additional conservation properties. For instance, some EP and ED schemes also imply the conservation of momenta, or are geometrically invariant [22,23]. In this work we propose a new generalized approach that is naturally amenable to the treatment of a larger class of problems. In particular, EP and ED schemes are presented for cables, beams (which in turn, provide the rigid body formulation), shells and finite deformation elasto-dynamics in a unified framework. These formulations cover most of the usual and not-so-usual multibody applications. Although the present formulation leads to discretizations that are slightly different from the ones presented in the previous papers, it has the advantage of being very general and does not require addressing the problem of parameterization of finite rotations, which are completely arbitrary.

This work is organized as follows. Section 2 presents the derivation of EP and ED schemes for a simple, yet important case: cable dynamics. The basic concepts underlying the derivation of the proposed algorithms are easily presented for the simple governing equations associated with cable dynamics. Next, in Section 3, general schemes are developed for the various flexible components of multibody systems. The cases of geometrically exact beams (Section 3.3) and shells (Section 3.4), and finite deformation elasticity (Section 3.5) are presented. The discretization of the forces of constraint is addressed in Section 4. The last section is devoted to the discussion of a number of numerical simulations of multibody systems.

2. Derivation of the energy preserving and decaying schemes for cables

In this section, the EP and ED schemes are derived for the cable dynamics problem. The basic procedure for the development of the proposed algorithms is presented in detail for this simple case that is also of importance, in its own right, for modeling multibody systems.

2.1. Cable dynamics

Consider a cable idealized as a line in space, as depicted in Fig. 2. A point P on the cable is identified by its curvilinear coordinate s, measured along the undeformed configuration of the cable. The position vector of point P is denoted $\underline{r} = \underline{r}(s)$. In the following, the components of all vectors are measured in the inertial

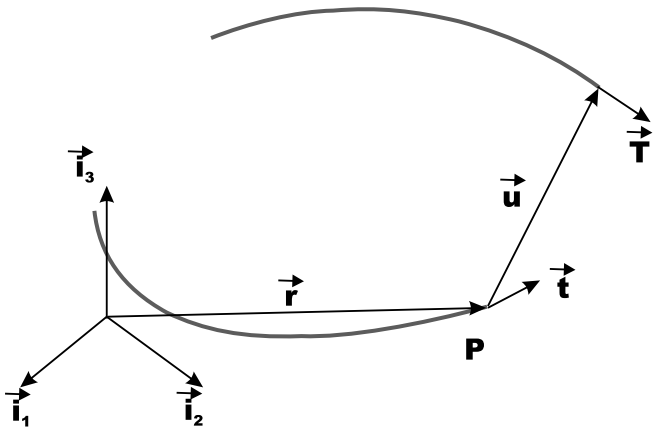

Fig. 2. Cable configurations before and after deformation.

system $\mathscr{S}$, defined by a triad of mutually orthogonal unit vectors $\vec{\imath}_1$, $\vec{\imath}_2$ and $\vec{\imath}_3$. The unit tangent vector to the cable at P is $\underline{t} = \underline{r}'$, where $(\cdot)'$ denotes a derivative with respect to s. After deformation, the position vector of point P becomes

$$\underline{R} = \underline{r} + \underline{u}, \tag{1}$$

where $\underline{u}$ is the displacement vector. The tangent to the cable in the deformed configuration is $\underline{R}' = \underline{r}' + \underline{u}'$. The axial strain in the cable is $e = 1/2(\mathrm{d}S^2 - \mathrm{d}s^2)/\mathrm{d}s^2$, where $\mathrm{d}S^2 = \mathrm{d}\underline{R} \cdot \mathrm{d}\underline{R}$, and can then be expressed as

$$e = \tfrac{1}{2}\underline{u}' \cdot \underline{u}' + \underline{r}' \cdot \underline{u}'. \tag{2}$$

For this case, the Principle of Virtual Work writes

$$\delta V = \int_L \int_\Omega \sigma \delta e \, \mathrm{d}\Omega \, \mathrm{d}s = \int_L f \delta \underline{u}' \cdot (\underline{u}' + \underline{r}') \, \mathrm{d}s, \tag{3}$$

where $f = \int_\Omega \sigma \, \mathrm{d}\Omega$ is the axial stress resultant in the cable. The constitutive law for the cable is $f = ke$, where k is its axial stiffness. The kinetic energy of the cable is expressed as

$$K = \frac{1}{2} \int_L \int_\Omega \rho \dot{\underline{u}} \cdot \dot{\underline{u}} \, \mathrm{d}\Omega \, \mathrm{d}s = \frac{1}{2} \int_L m \dot{\underline{u}} \cdot \dot{\underline{u}} \, \mathrm{d}s, \tag{4}$$

where m is the mass per unit length, and $\dot{(\cdot)}$ denotes a derivative with respect to time. For this problem, Hamilton's principle writes

$$\int_{t_\mathrm{i}}^{t_\mathrm{f}} \int_L (m \delta \underline{u} \cdot \dot{\underline{u}} + f \delta \underline{u}' \cdot (\underline{u}' + \underline{r}')) \, \mathrm{d}s \, \mathrm{d}t = 0, \tag{5}$$

and the governing equations of motion then follow

$$m \ddot{\underline{u}} - (f(\underline{u}' + \underline{r}'))' = \underline{0}. \tag{6}$$

2.2. The energy preserving scheme

A discretization of the cable equations of motion, Eq. (6), that implies a discrete conservation law for the total mechanical energy is now presented. The derivation starts by integrating by parts Hamilton's principle, Eq. (5), to find

$$\int_{t_\mathrm{i}}^{t_\mathrm{f}} \int_L (m \delta \underline{u} \cdot \ddot{\underline{u}} + f \delta \underline{u}' \cdot (\underline{u}' + \underline{r}')) \, \mathrm{d}s \, \mathrm{d}t = 0. \tag{7}$$

Times t_i and t_f denote the initial and final times for a time step, respectively, and the subscripts $(\cdot)_\mathrm{i}$ and $(\cdot)_\mathrm{f}$ indicate quantities at t_i and t_f, respectively. Furthermore, the subscript $(\cdot)_\mathrm{m}$ is used to denote mid-point average quantities defined as

$$(\cdot)_\mathrm{m} = \tfrac{1}{2}((\cdot)_\mathrm{f} + (\cdot)_\mathrm{i}). \tag{8}$$

Hamilton's principle, Eq. (7), is now approximated in time in the following manner

$$\Delta t \int_L \left(m(\underline{u}_\mathrm{f} - \underline{u}_\mathrm{i}) \cdot \frac{\dot{\underline{u}}_\mathrm{f} - \dot{\underline{u}}_\mathrm{i}}{\Delta t} + f_\mathrm{m}(\underline{u}'_\mathrm{f} - \underline{u}'_\mathrm{i}) \cdot (\underline{u}'_\mathrm{m} + \underline{r}') \right) \mathrm{d}s = 0. \tag{9}$$

Next, the strain increment between the initial and final time is evaluated as

$$e_\mathrm{f} - e_\mathrm{i} = (\underline{u}'_\mathrm{f} - \underline{u}'_\mathrm{i}) \cdot \underline{u}'_\mathrm{m} + \underline{r}' \cdot (\underline{u}'_\mathrm{f} - \underline{u}'_\mathrm{i}) = (\underline{u}'_\mathrm{f} - \underline{u}'_\mathrm{i}) \cdot (\underline{u}'_\mathrm{m} + \underline{r}'). \tag{10}$$

Furthermore, the discrete displacement field update is expressed in terms of the average velocities

$$\frac{\underline{u}_{\mathrm{f}} - \underline{u}_{\mathrm{i}}}{\Delta t} = \underline{\dot{u}}_{\mathrm{m}}. \tag{11}$$

Introducing Eqs. (10) and (11) into the approximate expression of Hamilton's principle, Eq. (7), then yields

$$\int_L \left(\frac{m}{2} (\underline{\dot{u}}_{\mathrm{f}} + \underline{\dot{u}}_{\mathrm{i}}) \cdot (\underline{\dot{u}}_{\mathrm{f}} - \underline{\dot{u}}_{\mathrm{i}}) + f_{\mathrm{m}} (e_{\mathrm{f}} - e_{\mathrm{i}}) \right) \mathrm{d}s = (K_{\mathrm{f}} + V_{\mathrm{f}}) - (K_{\mathrm{i}} + V_{\mathrm{i}}) = 0. \tag{12}$$

This statement implies the conservation of the total mechanical energy of the system over the time step.

The above developments suggest the following time-discrete equations of motion for the cable

$$m \frac{\underline{\dot{u}}_{\mathrm{f}} - \underline{\dot{u}}_{\mathrm{i}}}{\Delta t} - (f_{\mathrm{m}} (\underline{u}'_{\mathrm{m}} + \underline{r}'))' = \underline{0}, \qquad \underline{u}_{\mathrm{f}} = \underline{u}_{\mathrm{i}} + \Delta t \underline{\dot{u}}_{\mathrm{m}}, \tag{13}$$

where the mid-point values are given by Eq. (8). In view of Eq. (12), this form of the discrete equations clearly implies the preservation of the total mechanical energy of the system. Note that the spatial discretization of the equations has not been specified at this point: arbitrary discretizations will inherit the discrete energy preservation property.

2.3. The energy decaying scheme

As discussed in the introduction, energy preservation, per se, is not sufficient to yield robust time integration schemes. High frequency numerical dissipation must be added as an inherent feature of the scheme. Such a scheme is now constructed for the cable equations of motion using the EP scheme as a basic building block. An algorithmic parameter is introduced in the scheme to achieve a variable amount of high frequency numerical dissipation.

First, an additional state is introduced at time $t_j = \lim_{\epsilon \to 0} (t_{\mathrm{i}} + \epsilon)$, and the subscript $(\cdot)_j$ is used to denote quantities at this time. The following averages are now defined

$$(\cdot)_g = \tfrac{1}{2}((\cdot)_{\mathrm{f}} + (\cdot)_j), \qquad (\cdot)_h = \tfrac{1}{2}((\cdot)_j + (\cdot)_{\mathrm{i}}). \tag{14}$$

The ED scheme proceeds from the initial to the final time by means of two coupled steps: one step from t_{i} to t_{f}, the other from t_{i} to t_j. The time-discrete equations of dynamic equilibrium and their corresponding update relationships are given as

$$\begin{aligned}
&m \frac{\underline{\dot{u}}_{\mathrm{f}} - \underline{\dot{u}}_{\mathrm{i}}}{\Delta t} - (f_g (\underline{u}'_g + \underline{r}'))' = \underline{0}, \\
&m \frac{\underline{\dot{u}}_j - \underline{\dot{u}}_{\mathrm{i}}}{\Delta t} + \tfrac{1}{3}(f_g (\underline{u}'_g + \underline{r}') - f_p (\underline{u}'_h + \underline{r}'))' = \underline{0}, \\
&\underline{u}_{\mathrm{f}} = \underline{u}_{\mathrm{i}} + \frac{\Delta t}{2} (\underline{\dot{u}}_{\mathrm{f}} + \underline{\dot{u}}_j), \\
&\underline{u}_j = \underline{u}_{\mathrm{i}} - \frac{\Delta t}{6} (\underline{\dot{u}}_{\mathrm{f}} - \underline{\dot{u}}_{\mathrm{i}} - \alpha (\underline{\dot{u}}_j - \underline{\dot{u}}_{\mathrm{i}})),
\end{aligned} \tag{15}$$

where α is a tuning parameter that controls the amount of numerical dissipation provided by the scheme and the force f_p is given by

$$f_p = f_h + \alpha \frac{f_j - f_{\mathrm{i}}}{2}. \tag{16}$$

Hamilton's principle, Eq. (7), is used here again to prove the energy decay inequality implied by the proposed discretization

$$\int_L \left(m(\underline{u}_\mathrm{f} - \underline{u}_\mathrm{i}) \cdot \frac{\dot{\underline{u}}_\mathrm{f} - \dot{\underline{u}}_\mathrm{i}}{\Delta t} + f_g(\underline{u}'_\mathrm{f} - \underline{u}'_\mathrm{i}) \cdot (\underline{u}'_g + \underline{r}') + 3m(\underline{u}_j - \underline{u}_\mathrm{i}) \cdot \frac{\dot{\underline{u}}_j - \dot{\underline{u}}_\mathrm{i}}{\Delta t} - f_g(\underline{u}'_j - \underline{u}'_\mathrm{i}) \cdot (\underline{u}'_g + \underline{r}') \right.$$
$$\left. + f_p(\underline{u}'_j - \underline{u}'_\mathrm{i}) \cdot (\underline{u}'_h + \underline{r}') \right) \mathrm{d}s$$
$$= \int_L \left(\frac{m}{2}(\dot{\underline{u}}_\mathrm{f} \cdot \dot{\underline{u}}_\mathrm{f} - \dot{\underline{u}}_\mathrm{i} \cdot \dot{\underline{u}}_\mathrm{i}) + \alpha \frac{m}{2}(\dot{\underline{u}}_j - \dot{\underline{u}}_\mathrm{i}) \cdot (\dot{\underline{u}}_j - \dot{\underline{u}}_\mathrm{i}) + \frac{k}{2}(e_\mathrm{f}^2 - e_\mathrm{i}^2) + \alpha \frac{k}{2}(e_j - e_\mathrm{i})^2 \right) \mathrm{d}s$$
$$= (K_\mathrm{f} + V_\mathrm{f}) - (K_\mathrm{i} + V_\mathrm{i}) + \alpha c^2 = 0, \tag{17}$$

where c^2 is a positive quantity given by

$$c^2 = \frac{m}{2}(\dot{\underline{u}}_j - \dot{\underline{u}}_\mathrm{i}) \cdot (\dot{\underline{u}}_j - \dot{\underline{u}}_\mathrm{i}) + \frac{k}{2}(e_j - e_\mathrm{i})^2 \geqslant 0. \tag{18}$$

This result implies the decay of the total mechanical energy over one step of the algorithm, $(K_\mathrm{f} + V_\mathrm{f}) \leqslant (K_\mathrm{i} + V_\mathrm{i})$. The parameter α clearly controls the amount of energy that is dissipated within the step. Two such parameters could be used, controlling the amount of dissipated kinetic and strain energies, respectively, but this level of complexity does not seem to be necessary. Comparing the EP and ED schemes, Eqs. (13) and (15), respectively, it is clear that the ED scheme can be easily derived from the EP scheme. In other words, once an EP scheme is obtained, it can be readily generalized to an ED scheme to obtain the required high frequency numerical dissipation.

If the above ED scheme is applied to a single degree of freedom linear oscillator, the asymptotic spectral radius of the amplification matrix, ρ_∞, is found to be $\rho_\infty = (1-\alpha)/(1+\alpha)$. For $\alpha = 1$, $\rho_\infty = 0$, and asymptotic annihilation is achieved. If $\alpha = 0$, $\rho_\infty = 1$, and in view of Eq. (17), energy is exactly preserved. Hence, the ED scheme is in fact a family of schemes with a single tuning parameter, α, that controls the amount of high frequency numerical dissipation; both asymptotic annihilation or exact energy preservation can be achieved with the same scheme by using $\alpha = 1$ or 0, respectively. The spectral radius, algorithmic damping ratio and relative period error, as defined in Ref. [24], are plotted in Figs. 3–5 for varying α.

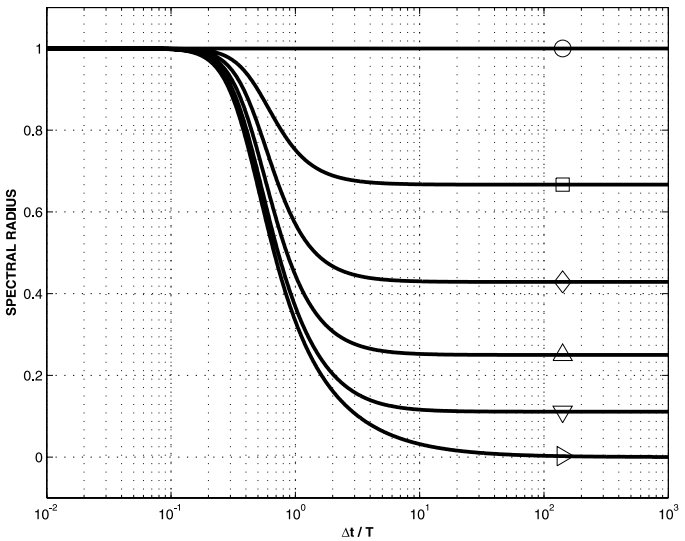

Fig. 3. Spectral radius of the ED scheme for varying α: (○) 0.0, (□) 0.2, (◇) 0.4, (△) 0.6, (▽) 0.8, (▷) 1.0.

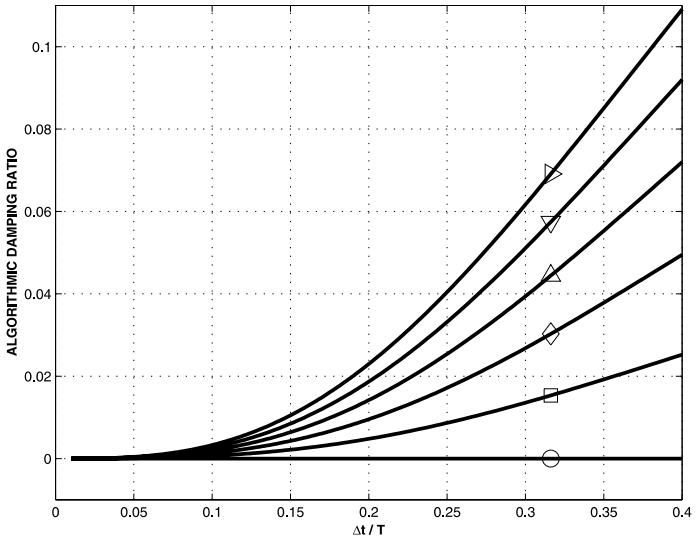

Fig. 4. Algorithmic damping ratio of the ED scheme for varying α: (○) 0.0, (□) 0.2, (◇) 0.4, (△) 0.6, (▽) 0.8, (▷) 1.0.

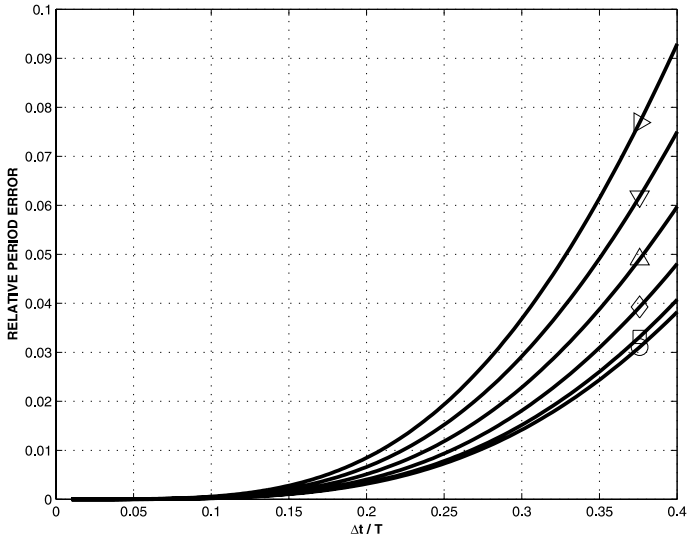

Fig. 5. Relative period error of the ED scheme for varying α: (○) 0.0, (□) 0.2, (◇) 0.4, (△) 0.6, (▽) 0.8, (▷) 1.0.

A simple inspection reveals that the EP stencil embedded in the ED scheme, Eq. (15), is different from that of the EP method described the previous section, Eq. (13). An error analysis based on Taylor series expansions for the linear harmonic oscillator model problem determined that the EP method is second order accurate, while ED($\alpha = 0$) is fourth order accurate. For the same model problem, ED($\alpha = 1$) is third order accurate. For general nonlinear problems, numerical experiments show that all methods exhibit convergence rates ranging between two and three. From a practical point of view, the ED scheme, with its ability to tune the amount of high frequency numerical dissipation, offers the advantage of requiring one single set of routines for each element in the library of a general computer code. When the EP version is

used, it is somewhat more expensive than using the EP scheme, due to the additional level of unknowns. However, implementation both the EP and ED schemes would require two sets of routines for each element, affecting code simplicity and maintenance.

3. Generalization to beams, shells and finite deformation elasticity

EP and ED schemes for cable dynamics were presented in the previous section. A similar approach will be followed to obtain robust integration schemes for dealing with geometrically exact beams and shells, as well as finite deformation elasticity. Since ED schemes can be readily constructed once the EP discretization is known, the sole EP schemes will be presented here, for brevity sake. At first, a general, unified formulation is developed that encompasses beams, shells, and finite deformation elasticity as special cases. The specific formulations for the three cases of interest are presented at the end of the section.

3.1. A general formulation

Consider the position vector of a material point P, denoted $\underline{r}$ and $\underline{R}$ in the reference and deformed configurations of the structure, respectively. In the case of beams and shells, this position vector will be given as the sum of two quantities: the position vector of a point on a reference entity, the reference curve for a beam or mid-surface for a shell, and the position vector of a material point with respect to this reference entity. This decomposition is a direct consequence of the usual kinematic assumptions associated with beam and shell theories: beam cross-sections remain plane and fibers normal to the shell plane remain straight lines. Such a decomposition is clearly not required for the case of finite deformation elasticity.

In the deformed configuration of the structure, the components of the position vector measured in $\mathscr{S}$ are

$$\underline{R} = \underline{r} + \underline{u} + E\underline{x}, \tag{19}$$

where $\underline{u}$ is the displacement vector. The matrix E stores the base vectors of the reference entity in the deformed configuration, denoted $\underline{E}_i$, $i = 1, 2, 3$, i.e.

$$E = [\underline{E}_1, \underline{E}_2, \underline{E}_3]. \tag{20}$$

Finally, the components of the 3×1 array $\underline{x}$ are either zero or the Lagrangian material coordinates x_i along the base vectors in the reference configuration. The actual components of $\underline{x}$ differ for beam, shells, and finite deformation elasticity.

The base vectors $G = [\underline{G}_1, \underline{G}_2, \underline{G}_3]$ of a material point in the deformed configuration then become

$$G = E + x^{\mathrm{T}}\nabla E, \tag{21}$$

where $\nabla E = [\underline{E}_{i,j}]$, and the notation $(\cdot)_{,j}$ indicates a derivative with respect to the material coordinate x_j. x is given by the tensor product of $x = \underline{x} \otimes I$, where I is the identity tensor.

The Green–Lagrange strains components now become

$$e = \tfrac{1}{2}(G^{\mathrm{T}}G - I) = \tfrac{1}{2}(E^{\mathrm{T}}E - I + E^{\mathrm{T}}x^{\mathrm{T}}\nabla E + \nabla E^{\mathrm{T}}xE + \nabla E^{\mathrm{T}}xx^{\mathrm{T}}\nabla E). \tag{22}$$

Virtual changes in the strain energy of the structure are given by

$$\delta V = \int_D \delta\overline{V}\,\mathrm{d}D = \int_D \delta e \cdot \tau\,\mathrm{d}D, \tag{23}$$

where $\delta\overline{V}$ is the virtual strain energy density, D the volume of the body, and τ the second Piola–Kirchhoff stress tensor. Introducing the strains, Eq. (22), and taking into account the symmetry of the stress tensor then yields

$$\delta\overline{V} = \delta G \cdot G\tau = \delta G \cdot \overline{F}, \tag{24}$$

where $\overline{F} = G\tau$. The existence of a strain energy density function $\overline{V}$ is postulated here, hence the constitutive laws are of the form $\tau = \partial\overline{V}/\partial e$. Some of the components of τ will be null for beams and shells.

The velocity vector of material point P is obtained by differentiating the position vector, Eq. (19), with respect to time, to find

$$\underline{v} = \dot{\underline{u}} + \dot{E}\underline{x}. \tag{25}$$

The kinetic energy of the system is now

$$K = \int_D \overline{K}\,\mathrm{d}D = \frac{1}{2}\int_D \rho\underline{v}\cdot\underline{v}\,\mathrm{d}D, \tag{26}$$

where $\overline{K}$ is the kinetic energy density. Introducing the velocity vector, Eq. (25) then yields

$$\overline{K} = \tfrac{1}{2}\rho(\dot{\underline{u}} + \dot{E}\underline{x})\cdot(\dot{\underline{u}} + \dot{E}\underline{x}). \tag{27}$$

Hamilton's principle now writes

$$\int_{t_\mathrm{i}}^{t_\mathrm{f}}\int_D (\delta\overline{K} + \delta\overline{V})\,\mathrm{d}D\,\mathrm{d}t = \int_{t_\mathrm{i}}^{t_\mathrm{f}}\int_D (\rho(\delta\underline{u} + \delta E\underline{x})\cdot(\ddot{\underline{u}} + \ddot{E}\underline{x}) + \delta G\cdot\overline{F})\,\mathrm{d}D\,\mathrm{d}t = 0, \tag{28}$$

which generalizes Eq. (7) for the cable problem. The equations of motion of the system could be derived from this principle by expressing the variations $\delta E\underline{x}$ in terms of a minimum set of independent parameters, three or two components of virtual rotation for the cases of beams and shells, respectively.

3.2. Energy preserving scheme

The proof of energy preservation closely follows that presented for the cable problem. The following matrix identity will be used extensively

$$A_\mathrm{f}^\mathrm{T}B_\mathrm{f} - A_\mathrm{i}^\mathrm{T}B_\mathrm{i} = (A_\mathrm{f} - A_\mathrm{i})^\mathrm{T}B_\mathrm{m} + A_\mathrm{m}^\mathrm{T}(B_\mathrm{f} - B_\mathrm{i}), \tag{29}$$

where the mid-point values are defined in Eq. (8). Hamilton's principle, Eq. (28), is now approximated in time in the following manner

$$\int_D \left(\rho((\underline{u}_\mathrm{f} - \underline{u}_\mathrm{i}) + (E_\mathrm{f} - E_\mathrm{i})\underline{x})\cdot\left(\frac{\dot{\underline{u}}_\mathrm{f} - \dot{\underline{u}}_\mathrm{i}}{\Delta t} + \frac{\dot{E}_\mathrm{f} - \dot{E}_\mathrm{i}}{\Delta t}\underline{x}\right) + (G_\mathrm{f} - G_\mathrm{i})\cdot G_\mathrm{m}\tau_a\right)\mathrm{d}D = 0. \tag{30}$$

The change in strain components from t_i to t_f is evaluated with the help of identity (29) to find

$$e_\mathrm{f} - e_\mathrm{i} = \tfrac{1}{2}((G_\mathrm{f} - G_\mathrm{i})^\mathrm{T}G_\mathrm{m} + G_\mathrm{m}^\mathrm{T}(G_\mathrm{f} - G_\mathrm{i})) = (G_\mathrm{f} - G_\mathrm{i})^\mathrm{T}G_\mathrm{m}. \tag{31}$$

Over one time step, the strain components can be approximated as $e(\eta) = e_\mathrm{m} + \eta(e_\mathrm{f} - e_\mathrm{i})/2$, where $\eta = 2(t - t_\mathrm{m})/\Delta t$ is the nondimensional time. If the strain energy density function $\overline{V}$ is viewed as a function of the scalar variable η, the mean value theorem then implies the existence of a $\hat{\eta} \in [-1, 1]$ such that

$$\overline{V}_\mathrm{f} = \overline{V}_\mathrm{i} + 2\frac{\partial\overline{V}}{\partial e}\bigg|_{\hat{\eta}}\frac{\mathrm{d}e}{\mathrm{d}\eta} = \overline{V}_\mathrm{i} + \tau_a\cdot(e_\mathrm{f} - e_\mathrm{i}). \tag{32}$$

This relationship defines the average second Piola–Kirchhoff stress tensor, $\tau_a = \partial\overline{V}/\partial e|_{\hat{\eta}}$. Combining this result with Eq. (31) then leads to

$$(G_\mathrm{f} - G_\mathrm{i})^\mathrm{T}G_\mathrm{m}\cdot\tau_a = (e_\mathrm{f} - e_\mathrm{i})\cdot\tau_a = \overline{V}_\mathrm{f} - \overline{V}_\mathrm{i}. \tag{33}$$

For many beam and shell problems, the strains in the structure can be assumed to remain small. In that case, the strain displacement relationship, Eq. (22) simplifies to

$$e = \tfrac{1}{2}(E^{\mathrm{T}}E - I + E^{\mathrm{T}}x^{\mathrm{T}}\nabla E + \nabla E^{\mathrm{T}}xE), \tag{34}$$

and the virtual strain energy density becomes

$$\delta\overline{V} = \delta E \cdot (E + x^{\mathrm{T}}\nabla E)\tau + \delta\nabla E \cdot (E + xE\tau). \tag{35}$$

For linear constitutive laws in the form $\tau = Ce$, where C is the stiffness matrix, the average stresses simply becomes $\tau_a = Ce_{\mathrm{m}}$. It can be readily shown that Eq. (33) also holds for small strains and this new definition of the average stress tensor.

In close analogy with the cable problem, see Eq. (11), the following configuration updates are now defined

$$\frac{\underline{u}_{\mathrm{f}} - \underline{u}_{\mathrm{i}}}{\Delta t} = \underline{\dot{u}}_{\mathrm{m}}, \qquad \frac{E_{\mathrm{f}} - E_{\mathrm{i}}}{\Delta t} = \dot{E}_{\mathrm{m}}. \tag{36}$$

Introducing Eqs. (33) and (36) into the approximate expression for Hamilton's principle, Eq. (30), then leads to

$$\begin{aligned}
&\int_D \left(\tfrac{1}{2}\rho(\underline{\dot{u}}_{\mathrm{m}} + \dot{E}_{\mathrm{m}}\underline{x}) \cdot ((\underline{\dot{u}}_{\mathrm{f}} - \underline{\dot{u}}_{\mathrm{i}}) + (\dot{E}_{\mathrm{f}} - \dot{E}_{\mathrm{i}})\underline{x}) + (\overline{V}_{\mathrm{f}} - \overline{V}_{\mathrm{i}})\right) \mathrm{d}D \\
&\quad = \int_D \left(\tfrac{1}{2}\rho(\underline{\dot{u}}_{\mathrm{f}} + \dot{E}_{\mathrm{f}}\underline{x}) \cdot (\underline{\dot{u}}_{\mathrm{f}} + \dot{E}_{\mathrm{f}}\underline{x}) - \tfrac{1}{2}(\underline{\dot{u}}_{\mathrm{i}} + \dot{E}_{\mathrm{i}}\underline{x}) \cdot (\underline{\dot{u}}_{\mathrm{i}} + \dot{E}_{\mathrm{i}}\underline{x}) + (\overline{V}_{\mathrm{f}} - \overline{V}_{\mathrm{i}})\right) \mathrm{d}D \\
&\quad = \int_D ((\overline{K}_{\mathrm{f}} - \overline{K}_{\mathrm{i}}) + (\overline{V}_{\mathrm{f}} - \overline{V}_{\mathrm{i}}))\,\mathrm{d}D = 0.
\end{aligned} \tag{37}$$

This result clearly implies the conservation of the total mechanical energy of the system within a step.

3.3. Specialization to beams

Fig. 6 depicts a beam of length L and cross-section Ω, in the undeformed and deformed configurations. At a generic point Q along the reference line of the beam, vectors $\vec{e}_2$ and $\vec{e}_3$ define the plane of the beam cross-section in the reference configuration. As a result of the classical hypothesis of undeformability of the cross-section, the base vectors in the deformed configuration, $\vec{E}_2$ and $\vec{E}_3$, remain mutually orthogonal unit vectors, while $\vec{E}_1$ is not unit nor is it orthogonal to $\vec{E}_2$ or $\vec{E}_3$, as axial and shearing strains develop during the deformation. This kinematic description of the problem implies

$$\underline{x} = \begin{Bmatrix} 0 \\ x_2 \\ x_3 \end{Bmatrix}. \tag{38}$$

The base vectors at the reference line of the beam are

$$E = [\underline{r}_{,1} + \underline{u}_{,1}, R\underline{e}_2, R\underline{e}_3], \tag{39}$$

where R denotes the components of the finite rotation tensor such that $\underline{E}_i = R\underline{e}_i$, $i = 2, 3$. Hence, $\underline{E}_2 \cdot \underline{E}_2 = 1$, $\underline{E}_3 \cdot \underline{E}_3 = 1$, and $\underline{E}_2 \cdot \underline{E}_3 = 0$. The virtual rotation vector is $\delta\psi \times = \delta R R^{\mathrm{T}}$, and allows expressing the variations $\delta E\underline{x} = \delta(R\underline{x})$ in terms of three independent parameters

$$\delta E\underline{x} = \delta\psi \times R\underline{x}. \tag{40}$$

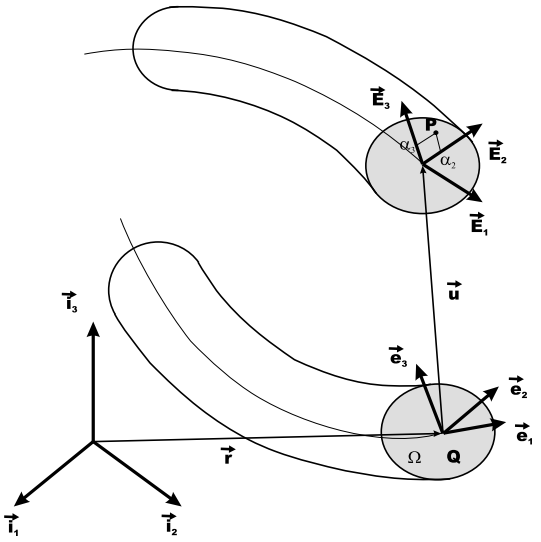

Fig. 6. Beam configurations before and after deformation.

Furthermore,

$$\nabla E = \begin{bmatrix} \underline{0} & \underline{0} & \underline{0} \\ \underline{E}_{2,1} & \underline{0} & \underline{0} \\ \underline{E}_{3,1} & \underline{0} & \underline{0} \end{bmatrix} \tag{41}$$

and the stress tensor becomes

$$\tau = \begin{bmatrix} \tau_{11} & \tau_{12} & \tau_{13} \\ \tau_{21} & 0 & 0 \\ \tau_{31} & 0 & 0 \end{bmatrix}. \tag{42}$$

The volume integrals are split into an integral over the cross-section Ω that leads to the definition of the classical sectional stress resultants, followed by an integral over the length of the beam:

$$\int_D \delta\overline{V}\,\mathrm{d}D = \int_L \left(\int_\Omega \delta\overline{V}\,\mathrm{d}x_2\,\mathrm{d}x_3 \right) \mathrm{d}s. \tag{43}$$

More details about the formulation of beam problems can be found in Refs. [8,11], and the generalization of the algorithm to ED schemes was presented in Refs. [16,18,19]. Although the algorithms presented in these various references are slightly different from the one presented here, they all share the same energy preservation/decay property. The primary differences between the various algorithms reside in the treatment of the finite rotations, as explained in Ref. [23]. The approach followed in the present paper demonstrates that the preservation of energy and the treatment of finite rotations are two entirely distinct problems. Rigid bodies can be treated in a manner identical to beams, simply ignoring the strain energy.

3.4. Specialization to shells

Fig. 7 depicts a shell of thickness h and reference surface Ω in the undeformed and deformed configurations. At a generic point Q on the mid-surface of the shell, vector $\vec{e}_3$ is normal to the mid-plane, and vectors $\vec{e}_1$ and $\vec{e}_2$ are tangent to the shell surface in the reference configuration. As a result of the classical hypotheses of undeformability of the normal fibers, the base vector in the deformed configuration, $\vec{E}_3$,

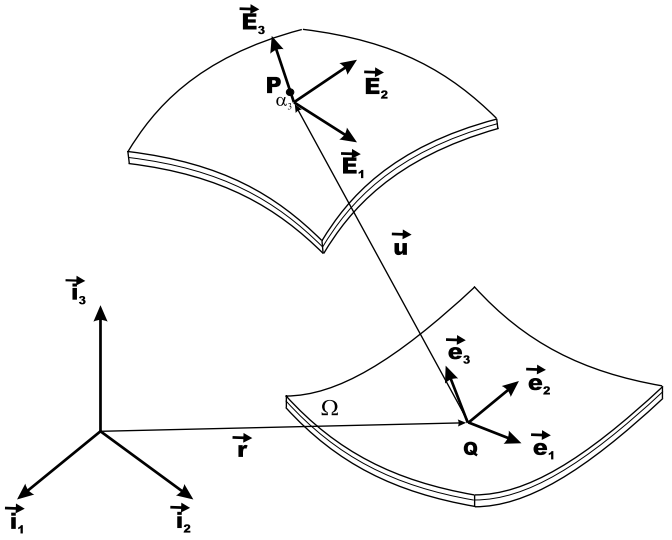

Fig. 7. Shell configurations before and after deformation.

remains a unit vector, while vectors $\vec{E}_1$ and $\vec{E}_2$ are not unit vectors nor are they orthogonal to $\vec{E}_3$, as axial and transverse shearing strains develop during the deformation. This kinematic description of the problem implies

$$\underline{x} = \begin{Bmatrix} 0 \\ 0 \\ x_3 \end{Bmatrix}. \tag{44}$$

The base vectors at the shell mid-plane are

$$E = [\underline{E}_1, \underline{E}_2, R\underline{e}_3], \tag{45}$$

where R denotes the components of the finite rotation tensor that brings $\vec{e}_3$ into $\vec{E}_3$. Hence, $\underline{E}_3 \cdot \underline{E}_3 = 1$. The finite rotation tensor R involves two independent parameters only, since drilling rotations about $\vec{E}_3$ are arbitrary. Update procedures can be developed for this problem, leading to five degree of freedom shell parameterizations. Consider the following partition of the rotation tensor: $R = [\beta, \underline{E}_3]$, where β is a 3×2 matrix. It is clear that

$$\delta\underline{E}_3 = \beta\delta\underline{q}, \tag{46}$$

where $\delta\underline{q}$ are the two independent parameters determining the orientation of the normal. Eq. (46) satisfies $\delta\underline{E}_3 \cdot \underline{E}_3 = 0$, a condition implied by the assumed inextensibility of the normal. Furthermore,

$$\nabla E = \begin{bmatrix} \underline{0} & \underline{0} & \underline{0} \\ \underline{0} & \underline{0} & \underline{0} \\ \underline{E}_{3,1} & \underline{E}_{3,2} & \underline{0} \end{bmatrix} \tag{47}$$

and the stress tensor becomes

$$\tau = \begin{bmatrix} \tau_{11} & \tau_{12} & \tau_{13} \\ \tau_{21} & \tau_{22} & \tau_{23} \\ \tau_{31} & \tau_{32} & 0 \end{bmatrix}. \tag{48}$$

The integral over the volume of the body is split in an integral through the shell thickness that leads to the definition of the classical stress resultants, followed by integral over the shell surface Ω:

$$\int_D \delta\overline{V}\,\mathrm{d}D = \int_\Omega \left(\int_h \delta\overline{V}\,\mathrm{d}x_3 \right) \mathrm{d}\Omega. \tag{49}$$

3.5. Specialization to finite deformation elasticity

In the case of finite deformation elasticity, no reference entity is needed, and hence

$$\underline{x} = \underline{0}. \tag{50}$$

Clearly, all the stress components are different from zero in this case.

More details about the formulation of finite deformation elasticity can be found in Ref. [10], and generalization of the algorithm to ED schemes was presented in Ref. [20].

4. Generalization to multibody systems

A distinguishing feature of multibody systems is the presence of a number of joints that impose constraints on the relative motion of the various bodies of the system. It is well known that the work done by the associated forces of constraint vanishes. In this paper, constraints will be enforced via the Lagrange multiplier technique and constraint forces will be discretized in a manner such that the work they perform exactly vanishes at the discrete solution level. In turns, this implies that the discrete energy preservation/decay laws proved for the flexible members of the system are not upset by the introduction of the constraints. Furthermore, the proposed discretization also implies the exact satisfaction of the nonlinear constraint manifold at discrete times, i.e. the constraint condition will not drift.

Most joints commonly used for practical applications can be modeled in terms of the so called *lower pairs* [25]: the revolute, prismatic, screw, cylindrical, planar and spherical joints. The kinematics of lower pair joints will be described in terms of two Cartesian frames $E^{\mathrm{A}} = [\underline{E}_1^{\mathrm{A}}, \underline{E}_2^{\mathrm{A}}, \underline{E}_3^{\mathrm{A}}]$ and $E^{\mathrm{B}} = [\underline{E}_1^{\mathrm{B}}, \underline{E}_2^{\mathrm{B}}, \underline{E}_3^{\mathrm{B}}]$, and two position vectors $\underline{R}^{\mathrm{A}} = \underline{r} + \underline{u}^{\mathrm{A}}$ and $\underline{R}^{\mathrm{B}} = \underline{r} + \underline{u}^{\mathrm{B}}$. $\underline{R}^{\mathrm{A}}$ and E^{A} represent the position and orientation of a point on a rigid or flexible body denoted body A, whereas $\underline{R}^{\mathrm{B}}$ and E^{B} are the corresponding quantities for body B. If the two bodies are rigidly connected to one another, their six relative motions, three displacements and three rotations, must vanish at the connection point. If one of the lower pair joints connects the two bodies, one or more relative motions will be allowed.

Let d_i be the relative displacement between the two bodies in the direction aligned with $\underline{E}_i^{\mathrm{A}}$, and θ_i the relative rotation about $\underline{E}_i^{\mathrm{A}}$. Table 1 then formally defines the six lower pairs in terms of the relative dis-

Table 1
Definition of the six lower pair joints

Joint type	Relative displacements			Relative rotations		
	d_1	d_2	d_3	θ_1	θ_2	θ_3
Revolute	No	No	No	No	No	Yes
Prismatic	No	No	Yes	No	No	No
Screw	No	No	$p\theta_3$	No	No	Yes
Cylindrical	No	No	Yes	No	No	Yes
Planar	Yes	Yes	No	No	No	Yes
Spherical	No	No	No	Yes	Yes	Yes

"Yes" or "No" indicate that the corresponding relative motion is allowed or inhibited, respectively. For the screw joint, p is the screw pitch.

placement and/or rotation components that can be either free or constrained to a null value. If the three components of relative displacement are inhibited, as is the case for the revolute and spherical joints, or if the three relative rotations are inhibited, as for the prismatic joint, the constraint equations are replaced within the finite element framework by the boolean identification of the corresponding degrees of freedom of the two bodies.

Each lower pair constraint can be expressed by one of the following two equations

$$\underline{E}_i^{\mathrm{A}} \cdot (\underline{u}^{\mathrm{A}} - \underline{u}^{\mathrm{B}}) - d_i = 0, \tag{51}$$

$$\cos\theta_i(\underline{E}_j^{\mathrm{A}} \cdot \underline{E}_k^{\mathrm{B}}) - \sin\theta_i(\underline{E}_k^{\mathrm{A}} \cdot \underline{E}_k^{\mathrm{B}}) = 0. \tag{52}$$

The first equation constrains the relative displacement if $d_i = 0$, whereas if d_i is a free variable it defines the unknown relative displacement in that direction. Similarly, the second equation either constrains the relative rotation if $\theta_i = 0$, or defines the unknown relative rotation θ_i if it is a free variable. The constraint conditions, Eq. (51) or (52), can be formally written as

$$\mathscr{C} = 0. \tag{53}$$

$\mathscr{C}$ is a linear combination of functions of the following type

$$D = g(r)(\underline{a} \cdot \underline{b}) + h(r), \tag{54}$$

where $\underline{a}$ and $\underline{b}$ indicate the vectors $\underline{E}_i$ or $\underline{u}$, $g(r)$ and $h(r)$ are two functions of r, and r denotes a relative motion variable, either d_i or θ_i. For example, for the first term of the relative displacement constraint, Eq. (51), $\underline{a} = \underline{E}_i^{\mathrm{A}}$, $\underline{b} = \underline{u}^{\mathrm{A}}$, $r = d_i$, $g(r) = 1$, and $h(r) = r$, while for the first term of the rotation constraint, Eq. (52), $\underline{a} = \underline{E}_j^{\mathrm{A}}$, $\underline{b} = \underline{E}_k^{\mathrm{B}}$, $r = \theta_i$, $g(r) = \cos\theta_i$ and $h(r) = 0$.

The virtual work done by the forces of constraint is

$$\delta W = \lambda \delta \mathscr{C}, \tag{55}$$

where λ is the Lagrange multiplier used to enforce the constraint $\mathscr{C} = 0$. $\delta\mathscr{C}$ can be expressed in terms of

$$\delta D = g(\underline{b} \cdot \delta\underline{a}) + g(\underline{a} \cdot \delta\underline{b}) + ((\underline{a} \cdot \underline{b})g' + h')\delta r, \tag{56}$$

where the notation $(\cdot)'$ indicates a derivative with respect to r.

The difference $D_{\mathrm{f}} - D_{\mathrm{i}}$ is now computed as

$$D_{\mathrm{f}} - D_{\mathrm{i}} = g_{\mathrm{m}}\underline{b}_{\mathrm{m}} \cdot (\underline{a}_{\mathrm{f}} - \underline{a}_{\mathrm{i}}) + g_{\mathrm{m}}\underline{a}_{\mathrm{m}} \cdot (\underline{b}_{\mathrm{f}} - \underline{b}_{\mathrm{i}}) + ((\underline{a} \cdot \underline{b})_{\mathrm{m}}g'_a + h'_a)(r_{\mathrm{f}} - r_{\mathrm{i}}), \tag{57}$$

where the subscript $(\cdot)_{\mathrm{m}}$ indicates the mid-point value as defined by Eq. (8). The quantities g'_a and h'_a are defined by the following relationships

$$g_{\mathrm{f}} - g_{\mathrm{i}} = g'_a(r_{\mathrm{f}} - r_{\mathrm{i}}), \quad h_{\mathrm{f}} - h_{\mathrm{i}} = h'_a(r_{\mathrm{f}} - r_{\mathrm{i}}) \tag{58}$$

and their existence is guaranteed by the mean value theorem. For instance, if $g(r) = \cos\theta$, standard trigonometric relationships imply

$$\cos\theta_{\mathrm{f}} - \cos\theta_{\mathrm{i}} = \frac{\sin\dfrac{\theta_{\mathrm{f}} - \theta_{\mathrm{i}}}{2}}{\dfrac{\theta_{\mathrm{f}} - \theta_{\mathrm{i}}}{2}} \cos\frac{\theta_{\mathrm{f}} + \theta_{\mathrm{i}}}{2}(\theta_{\mathrm{f}} - \theta_{\mathrm{i}}) = g'_a(\theta_{\mathrm{f}} - \theta_{\mathrm{i}}). \tag{59}$$

Introducing Eq. (57), the algorithmic virtual work over a time step can be evaluated as

$$W_{\mathrm{f}} - W_{\mathrm{i}} = \lambda_{\mathrm{m}}(\mathscr{C}_{\mathrm{f}} - \mathscr{C}_{\mathrm{i}}). \tag{60}$$

It is now clear that the work done by the discretized forces of constraint vanishes if $\mathscr{C}_{\mathrm{f}} - \mathscr{C}_{\mathrm{i}} = 0$. In order to avoid the drift phenomenon, it is preferable to enforce $\mathscr{C}_{\mathrm{f}} = 0$ at each time step, an equivalent condition. It is interesting to note that although the discretization of the equations of motion for elastic bodies

corresponds to an equilibrium of forces at t_m, see Eq. (13), the constraints are exactly satisfied at t_i and t_f, but not at t_m.

The proposed formulation is readily expanded to the ED scheme. In that case, a discretization is constructed that implies $W_f - W_i = \lambda_g(\mathscr{C}_f - \mathscr{C}_j) + \lambda_h(\mathscr{C}_j - \mathscr{C}_i)$, where λ_g and λ_h are two Lagrange multipliers. The work done by the forces of constraint is then made to vanish by imposing the two constraints $\mathscr{C}_f - \mathscr{C}_j = \mathscr{C}_j - \mathscr{C}_i = 0$. Here again, the drift phenomenon is avoided by imposing equivalent constraints, $\mathscr{C}_f = \mathscr{C}_j = 0$. More details about the treatment of constraints in ED schemes can be found in Ref. [17,21,22].

Many other types of constraints are found in multibody systems. For instance, sliding contact [26,27] and unilateral contact constraints involving rolling and friction [28,29] can be treated within the proposed framework. Note that nonholonomic constraints can also be treated in a similar manner, imposing the vanishing of work production over a time step.

5. Numerical examples

All the examples described in this section will be treated with the proposed ED family of schemes corresponding to values of the tuning parameter $\alpha \in [0, 1]$. Although any value of α within this range can be used, the examples described here will contrast the two extreme choices. For $\alpha = 1$ ($\rho_\infty = 0$), asymptotic annihilation is obtained, and this will be called the ED($\alpha = 1$) scheme. On the other hand, for $\alpha = 0$ ($\rho_\infty = 1$), exact energy preservation is achieved, and this will be called the ED($\alpha = 0$) scheme.

5.1. Lateral buckling of an I beam

If a beam is bent in its plane of greatest flexural rigidity, lateral buckling will occur when a critical value of the transverse load is reached. In this first example, the tip of a beam is subjected to a transverse load applied through a crank and link mechanism, as depicted in Fig. 8. The beam is clamped at one end, while the other end is connected to the link through a joint. Two different cases will be analyzed: in the first case, denoted *case 1*, a spherical joint connects the beam tip and the link, whereas in the second case, denoted

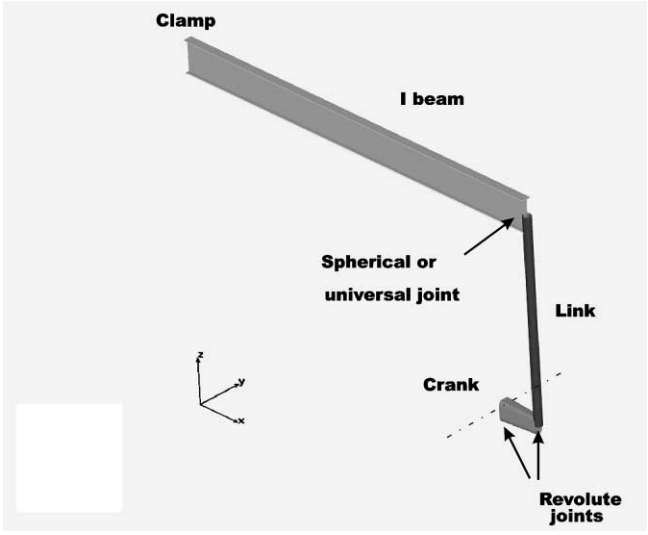

Fig. 8. Schematic of the lateral beam buckling problem.

case 2, this spherical joint is replaced by a universal joint. The crank and link are modeled by rigid bodies connected by revolute joints. As the crank rotates, the beam tip is pulled down, then up. Due to the system configuration, the vertical displacements imposed at the beam tip are different during the pull-up and pull-down phases. Since the actuation mechanism consists of rigid bodies, beam tip lateral motions are inhibited. When the buckling load is reached, the beam violently snaps laterally and becomes significantly softer in bending due to the pronounced twisting deformation.

The beam is of length $L = 1$ m and its I cross-section is of width $b = 20$ mm, depth $h = 80$ mm, and thickness $t = 2$ mm. Material properties are: modulus of elasticity $E = 210$ GPa, shearing modulus $G = 80$ GPa, and density $\rho = 7870$ kg/m^3. The crank and link length are $L_c = 0.1$ m and $L_l = 0.5$ m, respectively. The crank rotates at constant angular velocity $\omega = 1$ rad/s. The beam is modeled with three four-noded, geometrically exact beam elements, whose nonlinear features allow to capture the lateral buckling instability. The system is simulated for a period of 20 s, corresponding to slightly more than three complete crank revolutions.

5.1.1. Case 1: spherical joint connection

In case 1, the beam tip is connected to the actuation mechanism by means of a spherical joint. The simulation used the ED($\alpha = 1$) version of the proposed algorithm with a constant time step $\Delta t = 1 \times 10^{-03}$ s. This corresponds to about 15 steps per period of the beam first torsional mode that is severely excited at the onset of buckling. With such a time step, the ED scheme provides very little damping at the frequency of interest, whereas the higher vibration modes rapidly damp out due the high frequency numerical dissipation characteristics of the scheme. The EP version of the proposed algorithm was also exercised on this example but failed to converge soon after the first buckling event.

Fig. 9 depicts the post-buckling configurations of the beam at times $t = 1.04$ s and $t = 4.56$ s, respectively, which correspond to crank rotations of about 60° and 260°, respectively. Note the pronounced twisting of the beam, together with its large tip deflections.

Figs. 10 and 11 show the time histories of beam mid-point displacements and forces, respectively. Elastic vibrations are superposed onto the overall motion imparted by the crank. These vibrations are of significant amplitude and are violently excited at the onset of each buckling event. Note that the motion is not periodic, since the large amplitude vibrations initiate twisting of the beam one way or the other depending on the vibration pattern. Fig. 12 shows a detailed view of the response for the mid-point displacements

Fig. 9. Post-buckling configuration of the I beam (case 1) during the first pull-down and -up phases, left and right figures, respectively.

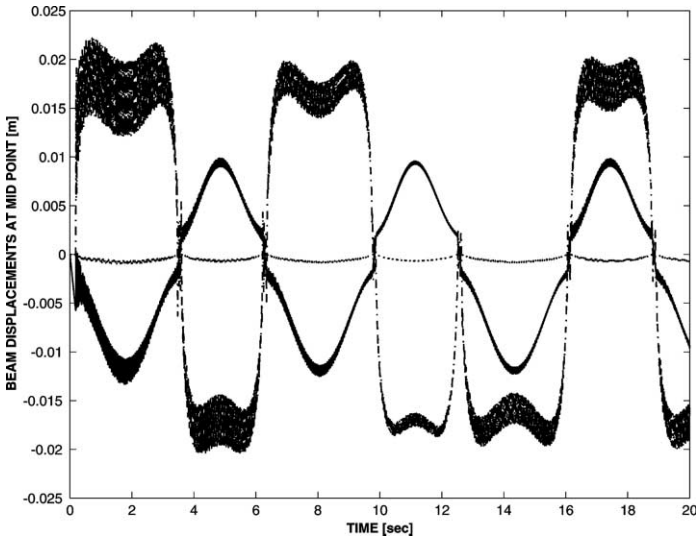

Fig. 10. Time history of the beam (case 1) mid-point displacements. x component: dotted line; y component: dash-dotted line; z component: solid line.

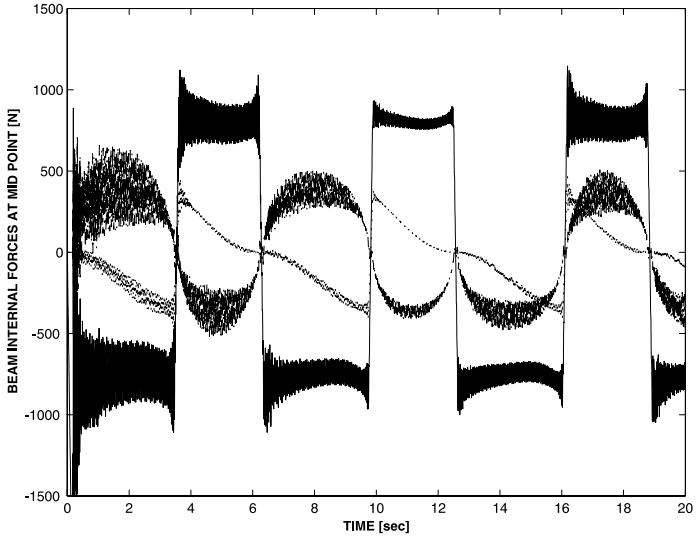

Fig. 11. Time history of the beam (case 1) mid-point internal forces. x component: dotted line; y component: dash-dotted line; z component: solid line.

during the onset of the fourth buckling event. The dotted line represents the foreshortening of the beam, a small quantity as compared to the other two displacement components. The lateral displacement component shown in dash-dotted line presents a vibratory pattern even in the unbuckled configuration of the beam. When the critical load is reached, the out-of-plane displacement increases dramatically. Finally, the solid line represents the vertical displacement of the beam mid-point. The linear response in the unbuckled regime is followed by highly vibratory behavior past the onset of buckling.

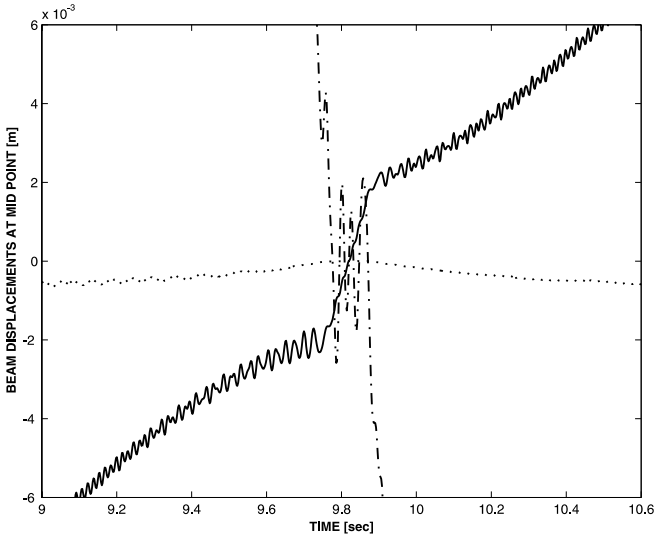

Fig. 12. Detail of the time history of the beam mid-point displacements, at the onset of the fourth buckling event (case 1). x component: dotted line; y component: dash-dotted line; z component: solid line.

5.1.2. Case 2: universal joint connection

In case 2, a universal joint connects the beam tip to the actuation mechanism. In the reference configuration, the universal joint allows rotations about axes $\vec{\imath}_1$ and $\vec{\imath}_2$, but inhibits those about the $\vec{\imath}_3$ axis. The damping characteristics of the universal joint are modeled by two rotational viscous dampers. The damping moments M_i are such that $M_i = c_i\dot{\theta}_i$, where $\dot{\theta}_1$ and $\dot{\theta}_2$ are the time rates of change of the two relative rotations at the joint, and $c_1 = c_2 = 0.1$ N m/(rad/s) the damping constants. These damping moments are discretized in such a manner that their work is a positive (i.e. dissipative) quantity within a step, in order to avoid upsetting the energy preservation/decay characteristics of the underlying algorithms. Here again a constant time step $\Delta t = 1 \times 10^{-03}$ s was used for the simulation.

At first, the proposed ED($\alpha = 1$) scheme was used for the simulation. Figs. 13 and 14 show the beam mid-point displacements and internal forces, respectively, whereas the relative rotations of the universal joint are depicted in Fig. 15. Here again, the beam first torsional mode is excited at the onset of each buckling event, but these oscillations rapidly decay due to the presence of dampers in the universal joint. After the first crank revolution, the solutions becomes nearly periodic.

Next the ED($\alpha = 0$) scheme was used for the simulation of this problem. The solution process failed to converge after about 1.28 s, soon after the first buckling event. The predictions of both ED($\alpha = 0$) and ED($\alpha = 1$) schemes are shown in Fig. 16 that depicts the mid-point displacements for the first 5 s of the simulation. The ED($\alpha = 0$) solution presents violent oscillations. The response of the beam mid-point internal forces, shown in Fig. 17, sheds additional light on the reason behind the failure of the solution process. The amplitudes of oscillations predicted by the ED($\alpha = 0$) scheme are *three to four orders of magnitude* greater than those predicted by the ED($\alpha = 1$) scheme. The Newton iteration process used for the solution of the nonlinear equations of motion is unable to deal with oscillations of such amplitude. This example clearly illustrates the shortcomings of the ED($\alpha = 0$) scheme: a robust integration scheme must present high frequency numerical dissipation characteristics to eliminate the high frequency oscillations inherent to the numerical solution of large sets of nonlinear equations. Even the presence of *physical damping* (as presented in case 2) does not alleviate the need for *high frequency numerical dissipation*.

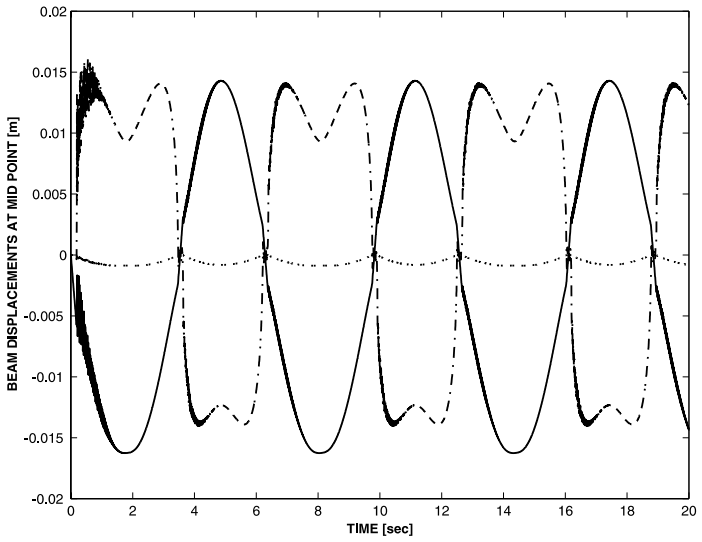

Fig. 13. Time history of the beam (case 2) mid-point displacements. x component: dotted line; y component: dash-dotted line; z component: solid line.

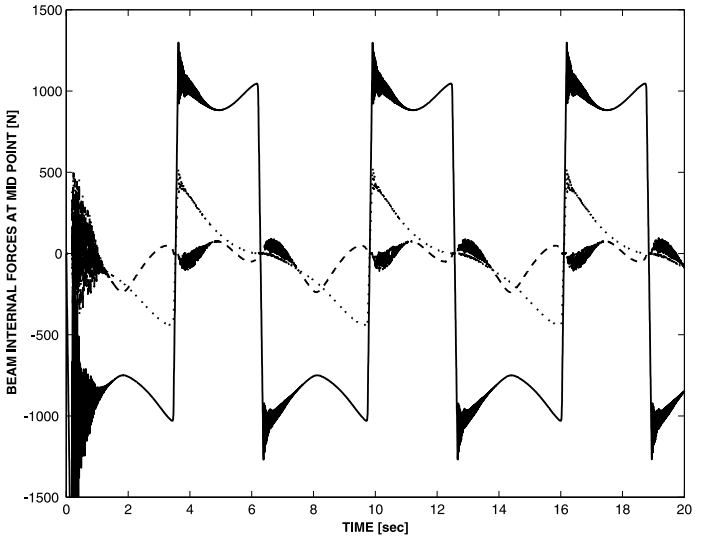

Fig. 14. Time history of the beam (case 2) mid-point internal forces. x component: dotted line; y component: dash-dotted line; z component: solid line.

5.2. The falling gate problem

The second example deals with the problem of a hinged gate falling under the effect of gravity, as depicted in Fig. 18. The gate of length $L = 4$ m is standing up against gravity and is connected to the ground by a revolute joint at point R. A rigid body of mass $M_T = 30$ kg is attached at the other end of the gate. At the gate mid-span, a rigid body of length $L_b = 0.4$ m connects the gate to a cable of length $L_c = 2$ m by means of a spherical joint at point A. The other end of the cable is connected to the ground at point B.

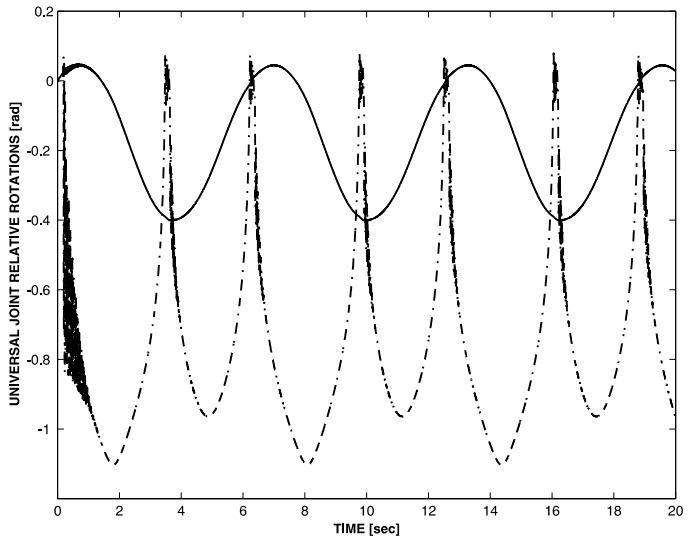

Fig. 15. Time history of the relative rotations at the universal joint (case 2).

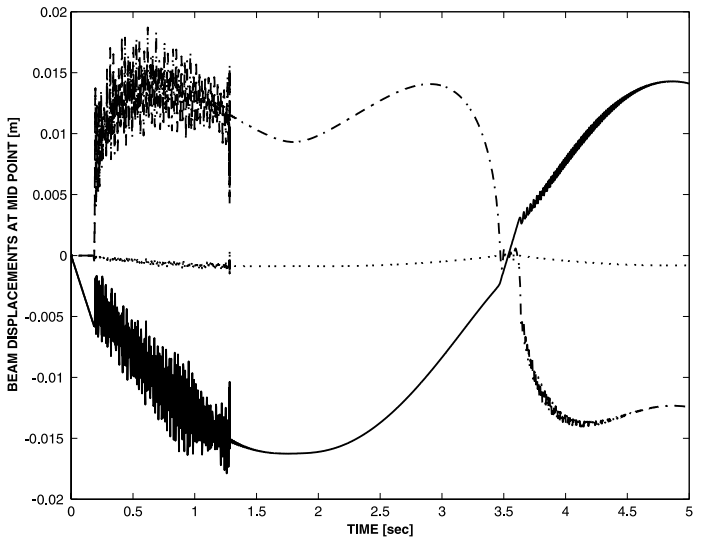

Fig. 16. Time history of the beam (case 2) mid-point displacements, for both the ED($\alpha = 0$) and the ED($\alpha = 1$) schemes. x component: dotted line; y component: dash-dotted line; z component: solid line.

The gate is modeled with six cubic beam element with the following properties: bending stiffnesses, $I_{22} = 300$ kN m^2 and $I_{33} = 23$ kN m^2, torsional stiffness $GJ = 12$ kN m^2, mass per unit span, $m = 1.60$ kg/m, and polar moment of inertia per unit span, $I_p = 0.01186$ kg m^2/m. The cable is modeled with eight cubic elements and has the following properties: axial stiffness, $k = 0.92$ MN, and a mass per unit span, $m = 3.4 \times 10^{-02}$ kg/m.

The ED($\alpha = 1$) scheme was used to simulate this problem with a constant time step $\Delta t = 1 \times 10^{-03}$ s for the first four seconds of the simulation, then switching to $\Delta t = 1 \times 10^{-04}$ s for the next half second. During

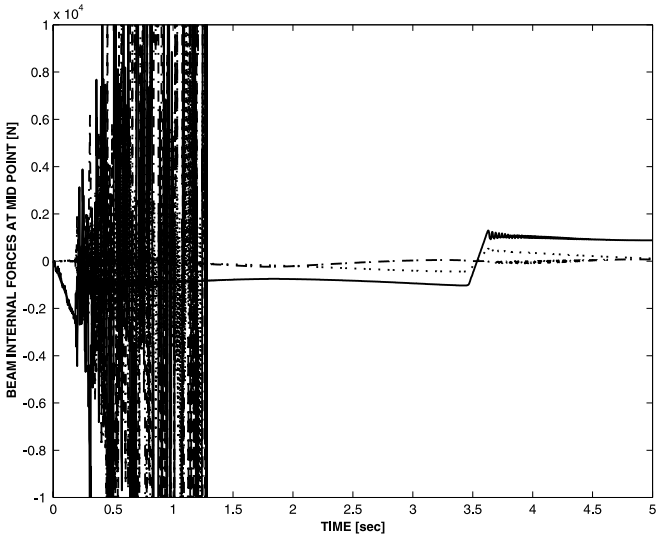

Fig. 17. Time history of the beam (case 2) mid-point internal forces, for both the ED($\alpha = 0$) and the ED($\alpha = 1$) schemes. x component: dotted line; y component: dash-dotted line; z component: solid line.

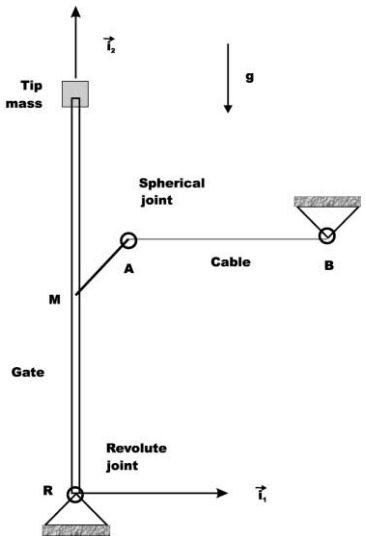

Fig. 18. Schematic of the falling gate problem.

the first phase of motion, lasting for about 4 s, the gate gently falls under the effect of gravity; all displacement, velocity, and internal force components are small and vary in a smooth manner. The second phase of the motion start at a time of about $t = 4.05$ s when the cable becomes taut and stops the gate fall. During this phase, that lasts for about half a second, forces of an impulsive nature are applied to the gate and cable, resulting in violent oscillations. The last phase of the motion starts at a time of about $t = 4.50$ s, when the cable is slack once again and the gate rebounds upward.

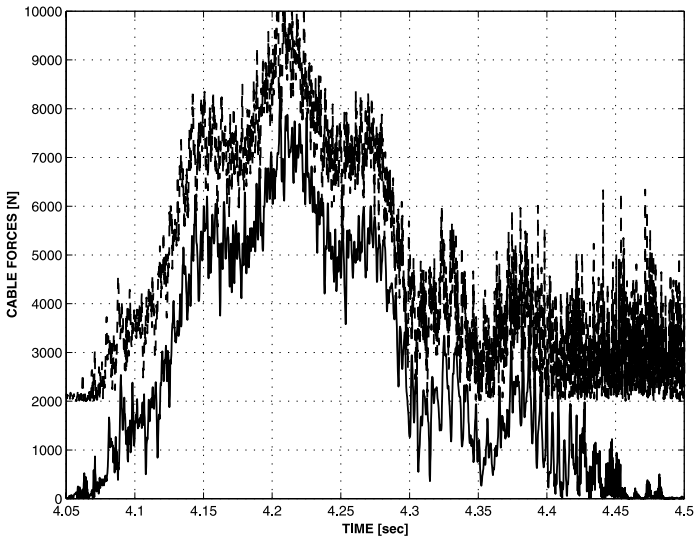

Fig. 19. Time history of the cable mid-point axial force for the ED($\alpha = 1$) (solid line) and ED($\alpha = 0$) (dotted line) schemes. For clarity, the curve for the ED($\alpha = 0$) scheme was moved up by 2000 N.

Fig. 19 show the time history of the cable mid-point internal force during the second phase of the motion as predicted by both ED($\alpha = 0$) and ED($\alpha = 1$) schemes. As the simulation proceeds, oscillations of increasing magnitude are observed for the ED($\alpha = 0$) scheme. Towards the end of this phase of motion, the forces predicted by the ED($\alpha = 1$) scheme rapidly vanish as the cable slackens. On the other hand the predictions of the ED($\alpha = 0$) scheme exhibit oscillations of increasing magnitude that have no physical meaning. The same information is presented in an alternate manner in Fig. 20 that depicts the discrete

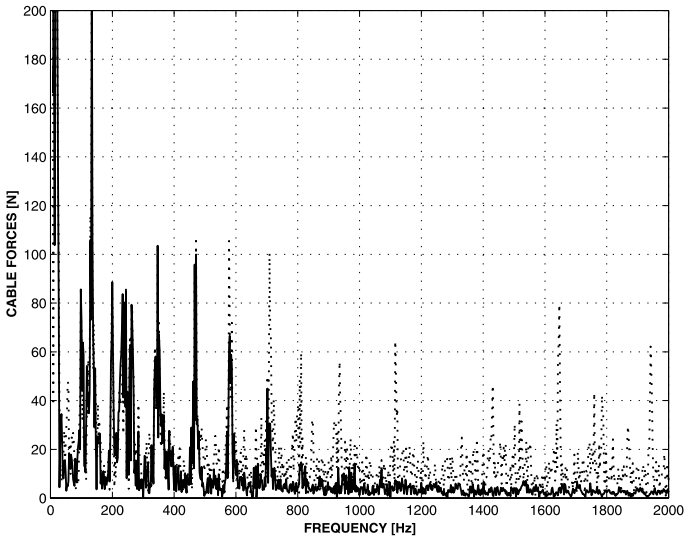

Fig. 20. Discrete Fourier transform of the cable mid-point axial force for the ED($\alpha = 1$) (solid line) and ED($\alpha = 0$) (dotted line) schemes.

Fourier transform of the time history shown in Fig. 19. The predictions of the ED($\alpha = 0$) and ED($\alpha = 1$) schemes are in close agreement for the low frequency components that contain the physically meaningful information about the behavior of the cable. The amplitudes of the high frequency components rapidly decay with increasing frequencies for the ED($\alpha = 1$) predictions due to the high frequency numerical dissipation characteristics of the algorithm. On the other hand, high frequency oscillation are present at all frequencies in the ED($\alpha = 0$) scheme predictions. Figs. 21 and 22 present the time history and discrete Fourier transforms of the gate mid-point velocities, respectively.

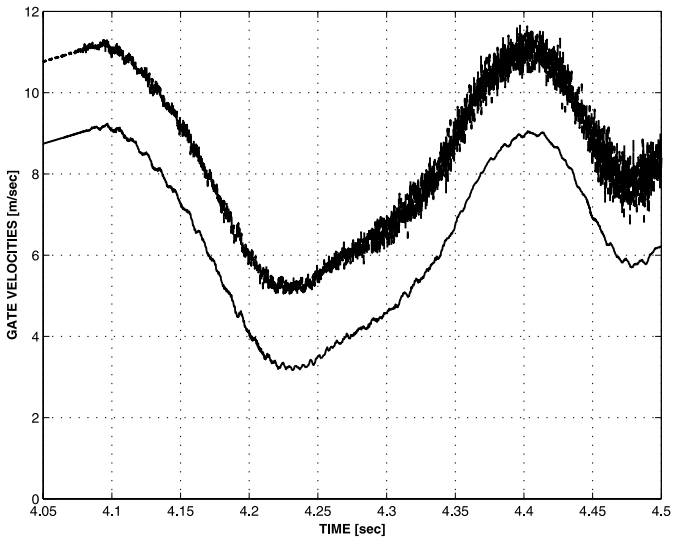

Fig. 21. Time history of the gate mid-point velocity for the ED($\alpha = 1$) (solid line) and ED($\alpha = 0$) schemes. For clarity, the curve for the ED($\alpha = 0$) scheme was moved up by 2 m/s.

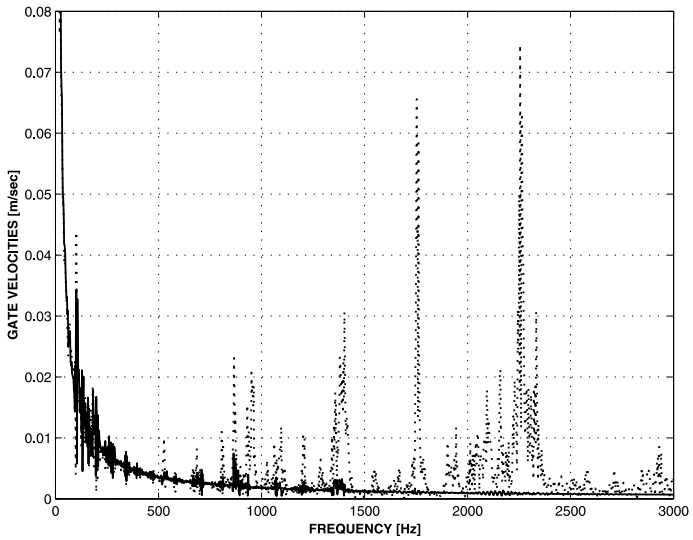

Fig. 22. Discrete Fourier transform of the gate mid-point velocity for the ED($\alpha = 1$) (solid line) and ED($\alpha = 0$) (dotted line) schemes.

6. Conclusions

In this work, a framework for the development of robust time integration schemes for nonlinear, flexible multibody systems was presented. The proposed algorithms are designed to meet four specific requirements: nonlinear unconditional stability, a rigorous treatment of all nonlinearities, the exact satisfaction of the constraints, and the presence of high frequency numerical dissipation. This methodology departs from the classical approach to time simulation whereby a suitable integrator is applied to the equations modeling the dynamics of multibody systems.

The proposed schemes are closely linked to the properties of the exact solution of the equations being integrated. Indeed, the most fundamental requirement, nonlinear unconditional stability, is achieved by enforcing the preservation of the total mechanical energy of the system and the vanishing of the work done by the forces of constraints at the discrete time level, two conditions that are satisfied at all times by the exact solution of the problem.

The indispensable high frequency numerical dissipation is obtained by proving an energy decay inequality, and the amount of numerical dissipation is controlled by a single parameter directly related to the spectral radius at infinity.

The proposed schemes can deal with general flexible nonlinear multibody systems and elasto-dynamics. Specific algorithms have been presented for cables, beams, shells, and elasto-dynamics. The kinematic nonlinearities are treated in a rigorous manner for all elements, and the material nonlinearities can be handled when the constitutive laws stem from the existence of a strain energy density function. The treatment of the constraint equations associated with the six lower pair joints have been presented as well.

The efficiency and robustness of the proposed approach were demonstrated with specific numerical examples.

References

[1] J.E. Shigley, J.J. Uicker, Theory of Machines and Mechanisms, McGraw-Hill, Inc., New York, 1980.
[2] E. Hairer, G. Wanner, Solving Ordinary Differential Equations II: Stiff and Differential-Algebraic Problems, Springer, Berlin, 1996.
[3] C.J. Budd, A. Iserles, Geometric integration: Numerical solution of differential equations on manifolds, Philosophical Transactions of the Royal Society of London Series A-Mathematical Physical and Engineering Sciences 357 (1999) 945–956.
[4] P. Lotstedt, L. Petzold, Numerical solution of nonlinear differential equations with algebraic constraints I: Convergence results for backward differentiation formulas, Mathematics of Computation 46 (1986) 491–516.
[5] P. Lotstedt, L. Petzold, Numerical solution of nonlinear differential equations with algebraic constraints II: Practical implications, SIAM Journal of Scientific and Statistical Computations 7 (1986) 720–733.
[6] T.J.R. Hughes, Stability, convergence, and growth and decay of energy of the average acceleration method in nonlinear structural dynamics, Computers and Structures 6 (1976) 313–324.
[7] J.C. Simo, K. Wong, Unconditionally stable algorithms for rigid body dynamics that exactly preserve energy and momentum, International Journal for Numerical Methods in Engineering 31 (1991) 19–52.
[8] J.C. Simo, N. Tarnow, M. Doblare, Non-linear dynamics of three-dimensional rods: Exact energy and momentum conserving algorithms, International Journal of Numerical Methods in Engineering 38 (1995) 1431–1473.
[9] J.C. Simo, N. Tarnow, A new energy and momentum conserving algorithm for the nonlinear dynamics of shells, International Journal for Numerical Methods in Engineering 37 (1994) 2527–2549.
[10] J.C. Simo, N. Tarnow, The discrete energy-momentum method. Conserving algorithms for nonlinear dynamics, ZAMP 43 (1992) 757–792.
[11] O.A. Bauchau, G. Damilano, N.J. Theron, Numerical integration of nonlinear elastic multi-body systems, International Journal for Numerical Methods in Engineering 38 (1995) 2727–2751.
[12] N.M. Newmark, A method of computation for structural dynamics, Journal of the Engineering Mechanics Division 85 (1959) 67–94.
[13] H.M. Hilber, T.J.R. Hughes, R.L. Taylor, Improved numerical dissipation for time integration algorithms in structural dynamics, Earthquake Engineering and Structural Dynamics 5 (1977) 282–292.

[14] J. Chung, G.M. Hulbert, A time integration algorithm for structural dynamics with improved numerical dissipation: The generalized-α method, Journal of Applied Mechanics 122 (1995) 254–266.
[15] A. Cardona, M. Géradin, Time integration of the equations of motion in mechanism analysis, Computers and Structures 33 (1989) 801–820.
[16] O.A. Bauchau, N.J. Theron, Energy decaying scheme for non-linear beam models, Computer Methods in Applied Mechanics and Engineering 134 (1996) 37–56.
[17] O.A. Bauchau, N.J. Theron, Energy decaying schemes for nonlinear elastic multi-body systems, Computers and Structures 59 (1996) 317–331.
[18] C.L. Bottasso, M. Borri, Energy preserving/decaying schemes for non-linear beam dynamics using the helicoidal approximation, Computer Methods in Applied Mechanics and Engineering 143 (1997) 393–415.
[19] C.L. Bottasso, M. Borri, Integrating finite rotations, Computer Methods in Applied Mechanics and Engineering 164 (1998) 307–331.
[20] O.A. Bauchau, T. Joo, Computational schemes for nonlinear elasto-dynamics, International Journal for Numerical Methods in Engineering 45 (1999) 693–719.
[21] O.A. Bauchau, Computational schemes for flexible, nonlinear multi-body systems, Multibody System Dynamics 2 (1998) 169–225.
[22] C.L. Bottasso, M. Borri, L. Trainelli, Integration of elastic multibody systems by invariant conserving/dissipating algorithms. Part I: formulation & Part II: numerical schemes and applications, Computer Methods in Applied Mechanics and Engineering 190 (2001) 3669–3733.
[23] O.A. Bauchau, C.L. Bottasso, On the design of energy preserving and decaying schemes for flexible, nonlinear multi-body systems, Computer Methods in Applied Mechanics and Engineering 169 (1999) 61–79.
[24] T.J.R. Hughes, Analysis of transient algorithms with particular reference to stability behavior, in: Computational Methods for Transient Analysis, North Holland, Amsterdam, 1983, pp. 67–155.
[25] J. Angeles, Spatial Kinematic Chains, Springer-Verlag, Berlin, 1982.
[26] O.A. Bauchau, On the modeling of prismatic joints in flexible multi-body systems, Computer Methods in Applied Mechanics and Engineering 181 (2000) 87–105.
[27] O.A. Bauchau, C.L. Bottasso, Contact conditions for cylindrical, prismatic, and screw joints in flexible multi-body systems, Multibody System Dynamics 5 (2001) 251–278.
[28] O.A. Bauchau, Analysis of flexible multi-body systems with intermittent contacts, Multibody System Dynamics 4 (2000) 23–54.
[29] O.A. Bauchau, On the modeling of friction and rolling in flexible multi-body systems, Multibody System Dynamics 3 (1999) 209–239.